Pertanika J. Sci. & Technol. 31 (S1): 59 - 85 (2023)

PERTANIKA JOURNALS

SCIENCE & TECHNOLOGY

Journal homepage: http://www.pertanika.upm.edu.my/

Development and Characterisation of Biocomposite Insulator Board from Durian Skin Fibres

Aisyah Humaira Alias[1], Edi Syams Zainudin[1,2]*, Mohd Nurazzi Mohd Norizan[3] and Ahmad Ilyas Rushdan[4]

[1]Advanced Engineering Materials and Composites Research Centre (AEMC), Department of Mechanical and Manufacturing Engineering, Faculty of Engineering, Universiti Putra Malaysia, 43400 Serdang, Selangor, Malaysia
[2]Institute of Tropical Forestry and Forest Products (INTROP), Universiti Putra Malaysia, 43400 Serdang, Selangor, Malaysia
[3]Bioresource Technology Division, School of Industrial Technology, Universiti Sains Malaysia, 11800 Penang, Malaysia
[4]Department of Chemical Engineering, Faculty of Chemical and Energy Engineering, Universiti Teknologi Malaysia, 81310 UTM Johor Bahru, Johor, Malaysia

ABSTRACT

Durian is Malaysia's most popular seasonal fruit, but less than half of the durian fruit is consumed as food. Durian is a type of fruit with a high percentage of waste, which becomes an environmental problem when discarded into the landfill site. Therefore, it is important to utilise durian waste as a potential natural fibre-based composite reinforcement. Durian skin residue is recognised as one of the potential lignocellulosic materials to replace wood in the insulation board industry. The present study aims to develop a low-cost insulation board using durian skin residues as reinforcing materials. Single-layer mats were manually formed, followed by hot pressing using polymeric methane diphenyl diisocyanate (PMDI) resin. The effect of different percentages of PMDI resin (0, 6, 8 and 10%) on the board's physical, mechanical, morphological, and thermal properties was investigated. It was found that 6% PMDI resin is the optimised resin amount to produce PMDI/durian skin fibre composite, and the board with 6% PMDI has the maximum static bending due to enhanced cross-linking by the fibre. In terms of thermal stability and conductivity, the incorporation of 6% of PMDI is considered the best formulation based on the value achieved. The overall results indicated that this study addresses a low-cost innovation for commercial insulation boards as it utilises durian waste and a low dosage of PMDI for implementation in the building and construction industry.

Keywords: Durian waste, insulation board, mechanical properties, physical properties, thermal properties

ARTICLE INFO

Article history:
Received: 06 March 2023
Accepted: 24 July 2023
Published: 27 October 2023

DOI: https://doi.org/10.47836/pjst.31.S1.04

E-mail addresses:
aisyah.humaira@upm.edu.my (Aisyah Humaira Alias)
edisyam@upm.edu.my (Edi Syams Zainudin)
mohd.nurazzi@usm.my (Mohd Nurazzi Mohd Norizan)
ahmadilyas@utm.my (Ahmad Ilyas Rushdan)
*Corresponding author

ISSN: 0128-7680
e-ISSN: 2231-8526

INTRODUCTION

Malaysia has a widely planted durian crop of up to 41%, or over 70,000 hectares (ha) of cultivated land (Zakaria, 2020). With such a large production of durian fruits in Malaysia, it is not inconceivable that this country will be affected by a high production of durian residues covering more than half of the fruit. Durian waste is estimated to be 60–70% of the durian fruit (Manshor et al., 2014). Approximately 40% of durian skin fibre (DSF) may be produced from 1 kg of durian skin residues, or 60–75% of DSF can be obtained from a single fruit. From the waste management perspective, excess durian skin residues can result in massive disposal costs, environmental problems, and odour and visual pollution (Adunphatcharaphon et al., 2020). The alternative approach is to recycle and raise the value of these durian residues into valuable products to lessen the amount of durian that goes to waste (E'Zzati et al., 2018). As a result of this initiative, the declining amount of organic waste disposed of will reduce environmental pollution.

In recent decades, DSF has been explored in many applications, such as a physical adsorbent, multi-mycotoxin binder, protective packaging, potential pharmaceutical applications, and components of building materials (Adunphatcharaphon et al., 2020; Ho & Bhat, 2015; Khedari et al., 2004; Payus et al., 2021; San Ha et al., 2020). For instance, DSF has been identified as a viable agricultural biofiller in the composites sectors due to its excellent physical properties, high crystallinity, biodegradable, renewable source, and low cost (Aimi et al., 2014; Manshor et al., 2014). Developing composite materials using DSF will add value to agricultural waste and minimise pollution by reducing organic waste (Aimi et al., 2014; Manshor et al., 2012). Also, Masrifah et al. (2021) transformed DSF into organic fertiliser for durian crops. The DSF was mixed thoroughly with dolomite before re-mixed with an effective microorganism 4 (EM4). The fermented results from converting durian skin waste into fertiliser can be directly harvested and utilised by farmers.

Due to the current focus on utilising available natural resources, this research focuses on using agricultural waste as reinforcement in composites (Azman et al., 2021). Biocomposites offer numerous benefits, making them an attractive choice in various industries (Sabaruddin et al., 2020). Firstly, they contribute to sustainability by utilising renewable resources such as plant-based fibres and biopolymers, reducing reliance on non-renewable fossil fuel-based materials. This eco-friendly approach helps lower the carbon footprint and promotes a more circular economy. Secondly, biocomposites can reduce weight due to the lightweight nature of natural fibres, leading to enhanced energy efficiency in applications like automotive and aerospace (Ali et al., 2015, 2018; Azammi et al., 2020). Additionally, the incorporation of natural fibres into a biopolymer matrix improves mechanical properties, including tensile strength, stiffness, and impact resistance, making biocomposites suitable for structural applications (Norfarhana et al., 2022; Shaker et al., 2020, 2022). Furthermore, biocomposites based on biopolymers can

be biodegradable, offering advantageous end-of-life options and waste management. The versatility of biocomposites allows for customisation and tailoring of properties to meet specific requirements, providing a wide range of applications. Overall, biocomposites offer sustainable, lightweight, mechanically enhanced, and customisable solutions that contribute to a greener future (Asyraf et al., 2022, Asyraf, Syamsir, et al., 2023 & Asyraf, Nurazzi, et al., 2023). Much research has been conducted on reinforcing natural fibre as filler in polymer to improvise biocomposites' mechanical and physical properties. This research examines composites' characteristics based on polymeric methane diphenyl diisocyanate (PMDI) reinforced with DSF. In this work, PMDI resin was reinforced with DSF in the form of particles to produce a low-cost insulation board. In order to produce a high-quality DSF/PMDI board at a reasonable cost, the physical and mechanical properties of the board with different resin contents (0, 6, 8 and 10%) will be evaluated and discussed in this study. The physical properties of the DS/PMDI board were investigated, where density and dimensional stability tests were used to characterise them. Meanwhile, the mechanical, thermal, and conductivity properties were also carried out. The study's primary objective was to identify the optimal resin content for DSF/PMDI boards with high strength, good dimensional stability, and better thermal properties.

MATERIALS AND METHODS

Materials

Durian skin waste was collected from a fruit stall in Selangor and shredded using a shredder machine, as shown in Figure 1, to produce durian skin particles with a range size of 1 x 2 cm^2. The particles were air-dried for a day and dried in the oven at 70°C until the moisture content (MC) reached 8–10%. The PMDI resin was provided by Evergreen Sdn. Bhd., Shah Alam, Selangor and used in the fabrication process of the boards.

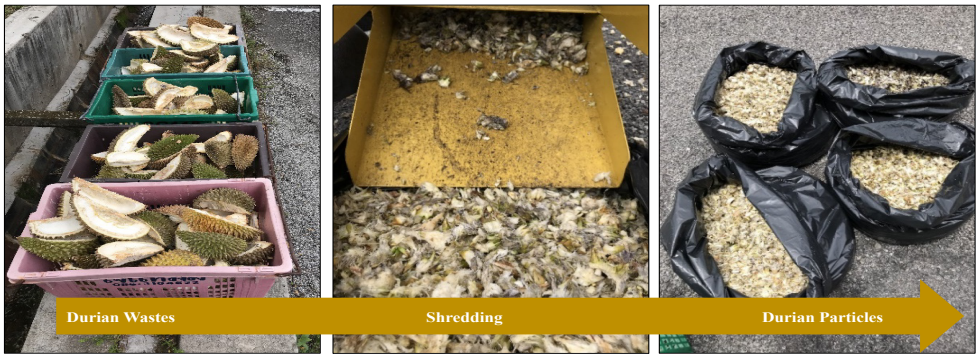

Figure 1. Durian wastes and durian particles

Methods

Fabrication of DSF/PMDI Board. The DSF-reinforced PMDI boards were produced by hot pressing using a manual hand lay-up technique. A specific amount of durian particles was weighed and placed in a rotary drum blender equipped with a pressurised spray nozzle, as shown in Table 1. The PMDI resin was sprayed onto the particles until the entire resin and the particles were blended uniformly. The furnish was collected, placed in a 350 × 350 mm square-shaped mould, and manually formed into a mat. The mats were cold-pressed at room temperature followed by hot-pressed at a pressure of 160 kg/cm² and a temperature of 190°C for 6 min using a computer-controlled press. The targeted density of the board was 0.60 g/cm³. Finally, the single-layer DSF/PMDI boards were conditioned at 23 ± 2°C and RH of 65 ± 5% until their equilibrium MC was obtained. The conditioning ensured that the resin in the board was cured uniformly.

Table 1
The formulations of the DSF-reinforced PMDI boards

Name of Composites	PMDI Resin (%)	PMDI Weight (g)	DSF Weight (g)
DSF/0PMDI	0	0	983.80
DSF/6PMDI	6	51.45	934.60
DSF/8PMDI	8	67.47	919.30
DSF/10PMDI	10	83.98	904.40

Preparation of Test Specimens

The samples were cut into specimens according to the ASTM D1895 (2003) and ASTM D1037 (2020), with 10 mm thickness. Table 2 shows the panel's dimensions for each test and the number of test specimens per board. The samples were then placed in the convection oven at 80°C for 24 h.

Table 2
Dimensions and number of test specimens

Test	Dimensions (mm)	Number of test specimens per board
Water Absorption (WA)	50 × 50	4
Thickness Swelling (TS)	50 × 50	4
Static Bending (SB)	200 × 50	3
Internal Bonding (IB)	50 × 50	4

Characterisation of Board Sample

Density. The DSF/PMDI board's density was determined by measuring each sample's mass and volume. The mass measurement was performed by digital precision balance, and dimensions measurement was performed using a vernier calliper. The density, ρ (g/cm^3), was then calculated according to ASTM D2395 (2022) at room temperature using Equation 1.

$$\rho = \frac{m}{V} \quad (1)$$

where m is the sample mass (g), and V is the sample volume (cm^3).

Dimensional Stability. The test specimens measured the initial weight and thickness using a digital precision balance and vernier calliper before being immersed in distilled water at room temperature according to ASTM D1037 (2020) Method B. The final weight and thickness were measured after 24 h. The percentage of water absorption (WA) was calculated using Equation 2.

$$WA = \frac{W_2 - W_1}{W_1} \times 100 \quad (2)$$

where W_1 is the weight of the sample before immersion (g), and W_2 is the weight of the sample after immersion in distilled water (g).

The percentage of thickness swelling (TS) was calculated using Equation 3.

$$TS = \frac{T_2 - T_1}{T_1} \times 100 \quad (3)$$

where T_1 is the thickness of the sample before immersion (mm), and T_2 is the thickness of the sample after water immersion (mm).

Static Bending. A three-point static bending test was conducted over a span length of 150 mm at 30 mm/min loading speed according to ASTM D1037 (2020) using the Tensile Machine model SHIMADZU AGS-X. The modulus of elasticity (MOE) value was calculated using Equation 4, and the modulus of rupture (MOR) value was calculated using Equation 5.

$$MOE = \frac{PL^3}{4fwt^2} \quad (4)$$

where f is the load-point deflection (mm).

$$MOR = \frac{3PL}{2wt^2} \quad (5)$$

where P is the maximum load at the point of delamination (N), L is the span length (mm), w is the width of the specimen (mm), and t is the thickness of the specimen (mm).

Internal Bonding. The internal bonding (IB) samples were glued to the heated metal blocks having a surface area of 50 × 50 mm with an epoxy resin. Another heated metal block with epoxy glue was placed on the other surface of the IB specimen. The specimens were kept in a conditioning room for 24 h before testing. All specimens were tested at a crosshead speed of 0.7 mm/min according to ASTM D1037 (2020) using an Internal Bonding Machine model LLOYD INSTRUMENT EZ20. The IB strength (N/mm^2) was calculated based on Equation 6.

$$IB = \frac{P'}{bl} \tag{6}$$

where *P'* is the maximum load (N) or force for the test specimen (N), *b* is the width of the test specimen (mm) and *l* = length of the test specimen (mm).

Scanning Electron Microscope (SEM). Scanning electron microscope (SEM) instrument model COMEX EM-30AX was used to observe the IB fracture surfaces of the test specimens to investigate the fracture mechanisms and interface adhesion of the board. The IB test samples were first cut (5 × 10 × 10 mm) at the fracture area before being placed in the SEM. The samples were then coated with gold to prevent the build-up of electron charge and to obtain a clear image of the samples. The magnification settings were set to 100x to investigate the detailed view of the fracture sample.

Thermogravimetric Analysis (TGA)

TGA was carried out using a TA Instruments TGA Q500 analyser in accordance with ASTM E1131 (2020) standards. About 8–10 mg of the composite was used for the TGA analysis. The samples were heated at 10°C per min from 25 to 570°C.

Differential Scanning Calorimetry Analysis (DSC)

The DSC analysis was conducted using a TA Instruments DSC Q1000 analyser according to ASTM D3418 (2021). About 7–9 mg of the composite was used for the DSC study. The glass transition and crystallisation temperatures were measured as functions of temperature in the range of 25–200°C with a heating rate of 10°C/min, and the results were recorded as a function of time.

Dynamic Mechanical Analysis (DMA)

TA instruments in New Castle, DE, USA, made a DMA called a Q800 that was used for the tests according to ASTM E1640 (2018). The specimens were cut at 60 mm (length) by 12 mm (wide) with a thickness of less than 6 mm. They were done at a frequency of 1 Hz

and a height of 30 m. All the specimens were first heated to 25°C in the DMA chamber. Then, dynamic heating scans were done from 25 to 120°C at a heating rate of 3°C/min.

Thermal Conductivity Measurement

Thermal conductivity measurements of each board used in this study were carried out using a NETZSCH HFM436 equipped with a ThermoCube cooling apparatus from Solid State Cooling Systems, USA. The thermal conductivity tests were performed according to the ASTM C518 (2021) standard. Each sample for the dimension of 300 × 300 mm^2 for each insulation board type was tested. The measurements were taken at an average temperature of 22.5°C. The temperature of the upper plate was set at 10°C, and the temperature of the lower plate was set at 35°C. The WinTherm32 software calculated the thermal conductivity, and the data was recovered when the system had reached equilibrium. Prior to conducting the tests, the specimens were conditioned to a moisture content average of 12 ± 3%.

RESULTS AND DISCUSSION

Density

The density of the board is one of the most significant elements of the properties of DSF/PMDI boards, such that by raising this factor, many of the functional aspects of boards are enhanced. The results in Figure 2 showed that the trend in density increased with the PMDI percentage. The density was, however, reduced when the resin content increased to 10%. In this comparison, the DSF/8PMDI board possessed the highest density of 0.581 g/cm^3, while the board without PMDI had the lowest density of 0.375 g/cm^3. The low density in DSF/0PMDI was due to the lack of interaction between DSF particles in the DSF/0PMDI board, as no resin filled the space between them. It eventually reduced the board's compatibility, resulting in a low density. The DSF/8PMDI board might have the highest density because the PMDI resin filled almost entirely the voids or spaces of the DSF particles, making the board less porous, more compact, and stronger. However, as the PMDI was increased to 10%, the density of the board was reduced (0.565 g/cm^3). It might be the consequence of an excessive amount of resin that demands a higher pressing temperature and longer pressing time to penetrate the resin into the voids of the particles (Kusumah et al., 2017).

Dimensional Stability

Water absorption (WA) is the DSF/PMDI board's ability to absorb water, whereas thickness swelling (TS) is the thickness change induced by soaking it in distilled water for 24 h. These tests measure the dimensional stability of the DSF/PMDI board, which impacts how a board product moves and distorts in service and its suitability for varied

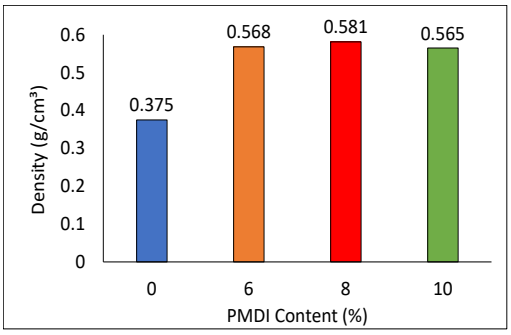

Figure 2. The density of the DSF/PMDI boards at different resin content

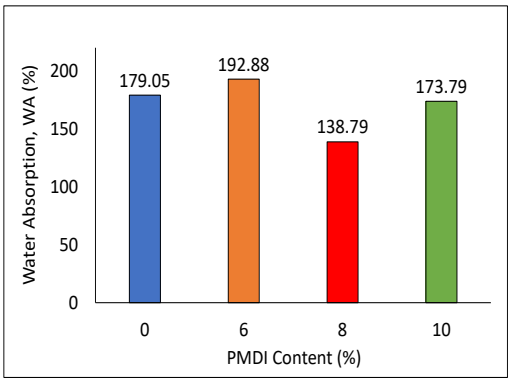

Figure 3. The water absorption of DSF/PMDI boards at different resin content

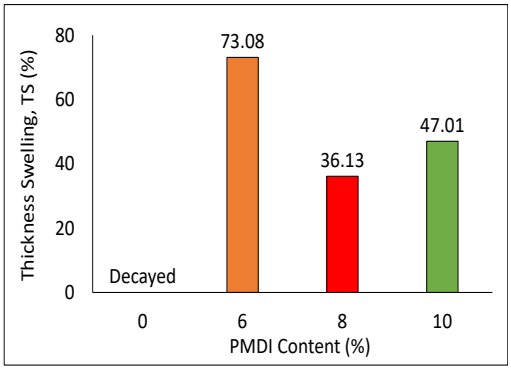

Figure 4. The thickness swelling of DSF/PMDI boards at different resin content

applications (Sargent, 2019). The results obtained in Figure 3 and Figure 4 showed similar trends in TS and WA. The results exhibited that the WA and TS decreased with the increase in resin content. In this comparison, the DSF/8PMDI board had the lowest WA and TS of 138.79% and 36.13%, respectively, whereas the DS/6PMDI board had the highest WA and TS of 192.88% and 73.08%, respectively. Lower WA and TS in the DSF/8PMDI board were found because of good adhesion between the DSF and PMDI. According to Saad and Kamal (2011), excellent chemical components in the resin were effectively cross-linking with the hydroxyl groups of the fibre, thus reducing the board's hygroscopicity.

In addition, due to the high density of the DSF/8PMDI board, the PMDI fills spaces in DSF, thus reducing void formation (Wong et al., 2000). In their study, a high-density board exhibited better flow and cross-linking, resulting in low void formation, less hygroscopic and more moisture resistant. It eventually reduced the water's ability to penetrate the board, resulting in less absorption. The DSF/8PMDI board also had higher PMDI content than the DSF/6PMDI board. A high PMDI content might cause low WA and TS as the PMDI have excellent water-repellence properties. Thus, the optimal PMDI resin was 8% because it had excellent dimensional stability.

Meanwhile, the DSF/6PMDI board had the highest percentage of WA and TS at 192.88% and 73.08%, respectively. Due to the small amount of resin utilised in developing the DSF/6PMDI board, the resin might not be enough to penetrate the particle surfaces

uniformly. It resulted in the greater existence of the void, which provided gaps that promote water absorption. Besides, the DSF/6PMDI board had low density. A study by Saad and Kamal (2011) discovered that a low-density board had a very porous structure that allowed water to penetrate the board and enhanced the WA rate, enabling the board to swell and thus increase the TS. Apart from that, DSF is hydrophilic, and PMDI is hydrophobic; therefore, water molecules penetrated the DSF when the board was wet, influencing fibre-resin interaction (Penjumras et al., 2015). According to a study by Alomayri et al. (2014), this penetration caused the fibre to absorb water and swell, causing micro-cracks that promote water capillarity and transport, allowing cellulose to absorb more water and penetrate the surface (Shaker et al., 2022).

On the other hand, the DSF/10PMDI board had high WA (173.79%) and TS (47.01%) due to the poor penetration and cross-link formation between the PMDI and DSF. According to a study by Liu et al. (2019), pressing at a higher temperature resulted in stronger interfacial adhesion and rapid thermal decomposition of hydrophilic components such as hemicelluloses. Therefore, higher pressing temperatures and time were required to achieve excellent adhesion in all layers of the DSF/10PMDI board (Kusumah et al., 2017). These high values may be related to the fact that no wax or other hydrophobic substance was used during particleboard manufacture. Water-repellent chemicals such as paraffin could be utilised in particleboard production to improve these properties.

Static Bending

The results in Figures 5 and 6 showed that the MOE trend is similar to MOR. In this comparison, the DSF/6PMDI board possessed the highest MOE and MOR at 2487.87 MPa and 8.53 MPa, respectively, while the DSF/0PMDI board had the lowest MOE and MOR of 165.05 MPa and 0.58 MPa, respectively. The low MOE value of the board indicated poor stiffness and rigidity performance, resulting in ductility and flexibility. While the low board's MOR indicated a lower ability to withstand the stresses applied perpendicular to its longitudinal axis. The value of MOE was increased from 165.05 to 2487.87 MPa, and MOR was increased from 0.58 to 8.52 MPa when the PMDI percentage in the DSF/PMDI board increased from 0 to 6%. The addition of PMDI greatly enhanced the MOE and MOR values since cross-linking between the DSF and PMDI improved the board's resistance to stress. This excellent adhesion prevented the DSF from shifting when the samples were subject to loading. It might be attributed to PMDI's effectiveness that coated the DSF particle surfaces and boosted chemical bonding via hydrogen bonds and polyurethane covalent bonds, as Saad and Kamal (2011) mentioned. In their findings, the isocyanate groups of PMDI reacted with water in the DSF particles, creating cross-linked polyureas for better mechanical bonding.

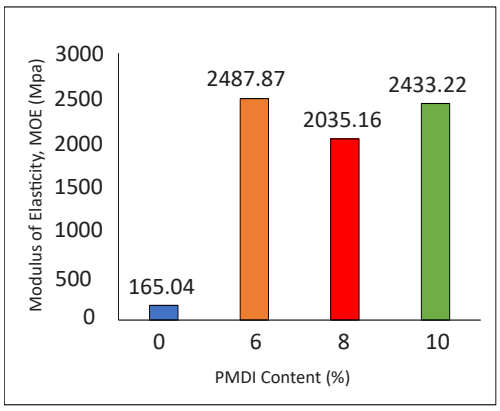

Figure 5. The MOE values of the DSF/PMDI boards at different resin content

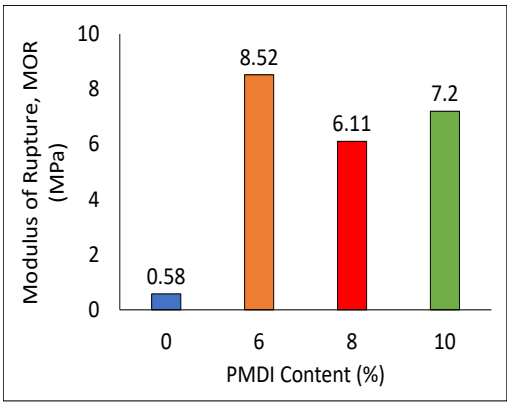

Figure 6. The MOR values of the DSF/PMDI boards at different resin content

However, the MOE and MOR decreased as the PMDI content increased from 6 to 8% to 2035.16 MPa and 6.11 MPa, respectively. Even though a DSF/8PMDI board had a high density and promoted better fibre-resin cross-link, a DSF/6PMDI board might contain more cellulose due to insufficient PMDI resin generated link with the cellulose fibre, as shown in SEM image analysis later. Higher cellulose content increased board stiffness, tensile, and impact strength. Way et al. (2013) reported a similar trend in mechanical properties, stating that additional fibre increased the board's mechanical properties due to fibre modulus being much higher than the PMDI. The study had also been supported by Alamri and Low (2012), in which cellulose fibres increased the fracture toughness of polymer matrices. In their study, increased fibre-rich areas indicated that stress was transferred from the resin to the fibres by absorbing more impact energy during fibre pull-out, breakage, and bridging, improving mechanical properties. The DSF/6PMDI had a higher presence of lignin than the DSF/8PMDI. According to Sahoo et al. (2011), adding lignin reduced the impact strength of composites because it acts as an adhesion promoter. Thus, the DSF/PMDI board with 6% had the optimal PMDI content due to its excellent MOE and MOR, with the highest stiffness and deformation resistance.

MOE and MOR improved when PMDI content was increased from 8 to 10% at 2433.22 MPa and 7.2 MPa, respectively. DSF/8PMDI exhibited poor MOE and MOR that might be due to bonding and fibre breaking, as Nazri et al. (2014) mentioned. Their research observed that the bond breakage was generated by the transmitted load surpassing the bond strength between the fibre-resin surface. Meanwhile, the fibre breakage was caused by the transmitted load surpassing the fibre strength and may have separated the fibres from the resin. However, DSF/10PMDI was lower than DSF/6PMDI, possibly due to the resin-rich region. According to Alamri and Low (2012), resin-rich regions indicated a lack of fibres that carried the transferred load from the resin, resulting in significant localised strains and thus having poor mechanical properties.

Internal Bonding

The results in Figure 7 show that the trend in IB increased with respect to their adhesive percentage. In this comparison, the DSF/10PMDI board possessed the highest IB, 0.612 MPa, while the DSF/0PMDI board had the lowest IB, 0.016 MPa. The increase in IB from 0 to 6% PMDI resulted from adding PMDI resin to the board, which promoted better interfacial bonding between fibres. Additionally, the density of the DSF/6PMDI board was higher than the DS/0PMDI board. High density indicated that the DSF/6PMDI board was less porous and void than the DSF/0PMDI board. The voids caused the inter-fibre bonding to be less effective (Jani & Izran, 2013). In the DSF/6PMDI board, the NCO group in PMDI resin reacted with water and OH groups in the DSF, forming a cross-link of carbon dioxide, amine, and polyurethane. In addition, the hydrogen bond further reacted with polyurethane, forming a rigid polar network and thus enhancing the chemical bonding of the composite. Therefore, it increases the ability to resist the pulling force in the DSF/6PMDI board (Jani & Izran, 2013).

It was noted that the IB of the DSF/6PMDI board was better than those of the DSF/8PMDI board. As mentioned before, although DSF/8PMDI board has a higher density, DSF/6PMDI board contains more lignin, which serves as an extra cross-linking agent by providing phenolic groups for the reaction with PMDI (Ostendorf et al., 2021). In their investigation, the phenolic groups provided by the kraft lignin function as extra cross-linking agents in the reaction with PMDI. Lignin is also a fibre-binding agent (Mossello et al., 2010). Therefore, the DSF/6PMDI board has a higher IB (0.471 MPa) than the DSF/8PMDI board.

The IB of the DSF/PMDI board was found to increase drastically as the resin percentage increased from 8 to 10%, eventually having it as the highest IB among the others (0.612 MPa) because a higher amount of resin promoted better interfacial bonding between fibres in the boards, prolonging the ability to withstand the pulling force generated by the test. A study by Saad and Kamal (2011) discovered that for PF-bonded boards, improvements were observed for IB at resin loadings of 9% and 11%, respectively, compared to 7%. They conclude that higher resin amounts promoted better interfacial adhesion between board particles, boosting the boards' ability to withstand the pulling force. Another factor to support the increase in IB of DSF/10PMDI might be the thick resin that has developed on the surface of the DSF. This thick resin remained on the surface and boosted the IB since PMDI

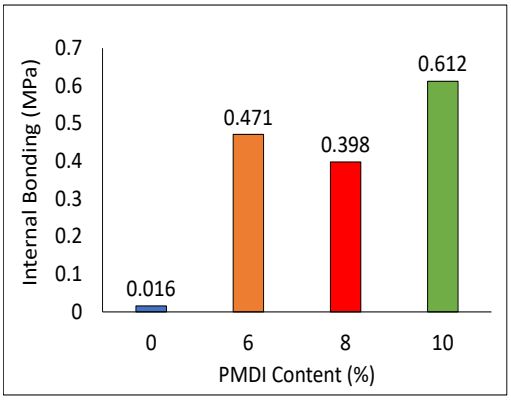

Figure 7. The IB of the DSF/PMDI board at different resin content

is known for its excellent bonding strength. Therefore, the DSF/10PMDI board had the highest IB.

A scanning electron microscope (SEM) was used to determine the fracture of the IB damage in more detail. In this study, the cross-sectional observation of the fracture from the testing was magnified up to 100x to focus on the fibre–matrix interfacial, matrix crack, and void content. Figure 8 shows the SEM micrograph of the DSF/PMDI board.

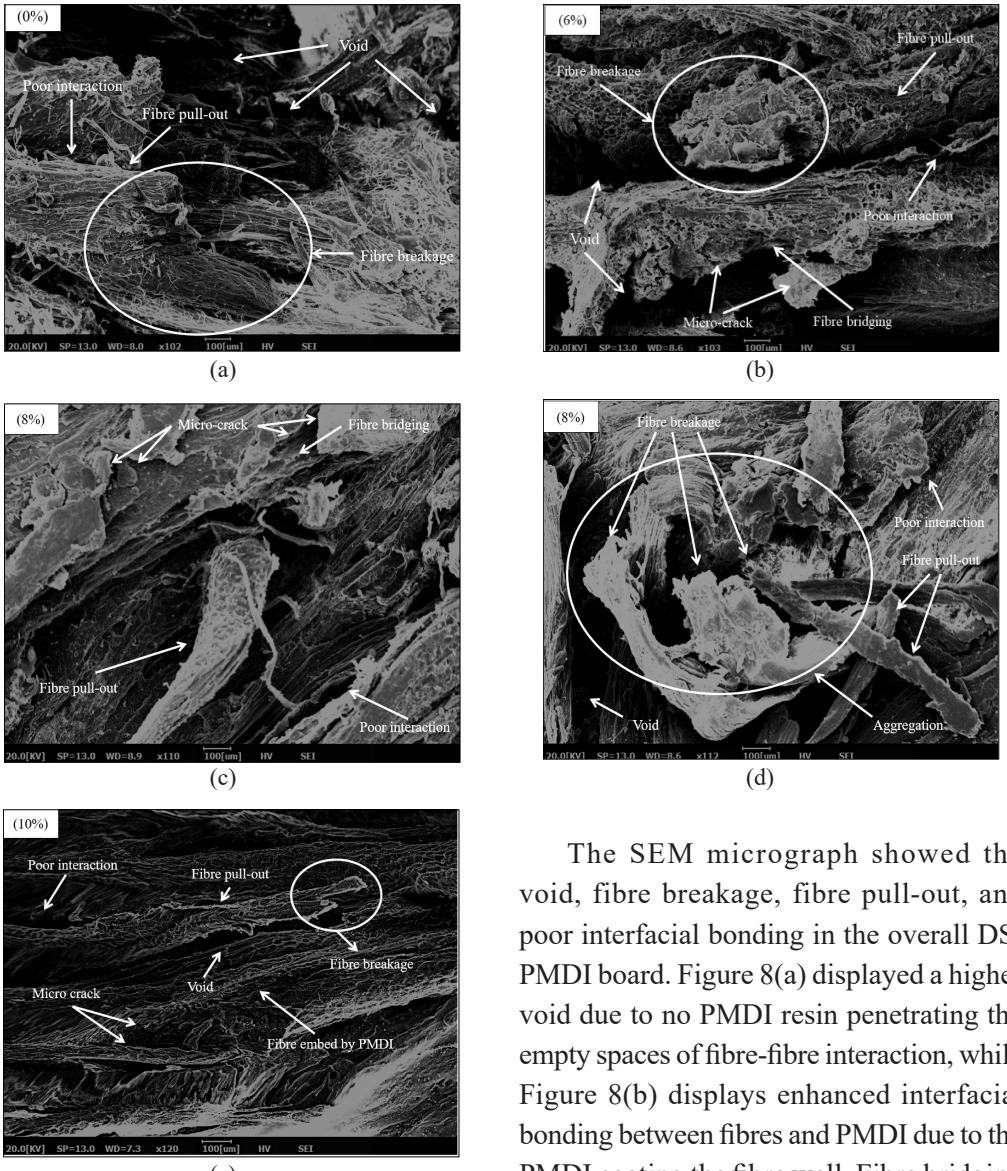

Figure 8. The SEM micrograph images of the DSF/PMDI board at (a) 0, (b) 6, (c–d) 8 and (e) 10% of PMDI

The SEM micrograph showed the void, fibre breakage, fibre pull-out, and poor interfacial bonding in the overall DS/PMDI board. Figure 8(a) displayed a higher void due to no PMDI resin penetrating the empty spaces of fibre-fibre interaction, while Figure 8(b) displays enhanced interfacial bonding between fibres and PMDI due to the PMDI coating the fibre well. Fibre bridging was visible, and the linked fibres between the top and lower layers of the crack plane

inhibited crack development and reduced crack propagation (Yousefi et al., 2016). There was also evidence of fibre breakage and pull-out, indicating that considerable energy was used to break and pull out the fibres, increasing the IB. The PMDI was also can be seen distributed evenly on the DSF surfaces. This adhesion secured the DSF and prevented movement during the IB test (Ibraheem et al., 2011). Their study discovered that kenaf fibres were held by polyurethane better under loading due to good adhesion. Thus, it is evident that the optimal PMDI content was 6% due to excellent morphological behaviour.

Figure 8(c–d) displays a higher number of micro-cracks, uncoated fibre on the fibre-resin surface, and voids, indicating poor adhesion between the DSF and PMDI. An increased number of micro-cracks in the PMDI resulted in fibre delamination. Fibre breakage and pull-out worsened because of the delamination, which separated it from PMDI (Yousefi et al., 2016). A high area of micro-cracks in Figure 8(e) and a high area of uncoated fibre in Figure 8(d) indicated that the DSF/8PMDI board had bad curing. It might be due to a lack of pressing time and temperature during the hot-pressing process, resulting in the DSF and PMDI being left in bulk. It also revealed that the aggregation of the DSF might result from the DSF being pulled out from the PMDI resin. It eventually caused a fibre transition, increased void, and poor interfacial adhesion (Yuan et al., 2019).

Furthermore, Figure 8(e) showed that the high IB measured by DSF/10PMDI may be attributed to the thick PMDI resin staying on the surface, causing PMDI-embedded fibre and low void formation. A low void formation increased the DS/PMDI board's mechanical properties, as Ibraheem et al. (2011) mentioned. According to their research, voids have a negative impact on mechanical properties, behave as defects, and enhance the formation and propagation of cracks.

Thermogravimetric Analysis

Based on all the TGA graphs in Figure 9, it can be said that the trend of the profiles for TGA is almost similar even though they were incorporated with different compositions of PMDI resin. The profiles for all samples show a double weight loss step, which occurred at approximately 43–45°C and 255–262°C. Table 3 shows the summary of the TGA test for the composites. T_{1onset} indicates the first onset degradation temperature, T_{1peak} indicates the first peak degradation temperature, T_{2onset} indicates the second onset degradation temperature, T_{2peak} indicates the first peak degradation temperature, $W_{minorloss}$ indicates the percentage for minor weight loss, and $W_{majorloss}$ indicates the percentage for major weight loss.

Weight loss that happened at approximately 100°C may be related to the elimination of water from the composites, and degradation at the starting temperature may also be related to the breaking of weak ether bonds between lignin units (-O-4 linkage) (Sahoo et al., 2011). Specifically, this showed that the weight loss in composites is related to the heat generated during water vaporisation. It has been broadly observed that the primary

Table 3
Summary of TGA test for the DSF/PMDI boards

Sample	T_{1onset} (°C)	T_{1peak} (°C)	$W_{minorloss}$ (%)	T_{2onset} (°C)	T_{2peak} (°C)	$W_{majorloss}$ (%)	Char Residue at 580°C (%)
DSF/0PMDI	43.98	60.71	8.71	263.28	308.98	58.64	30.52
DSF/6PMDI	43.88	59.79	7.33	255.86	304.45	57.33	31.60
DSF/8PMDI	43.11	58.41	8.58	259.27	305.98	58.68	30.72
DSF/10PMDI	44.38	59.07	7.21	258.25	305.42	58.56	30.80

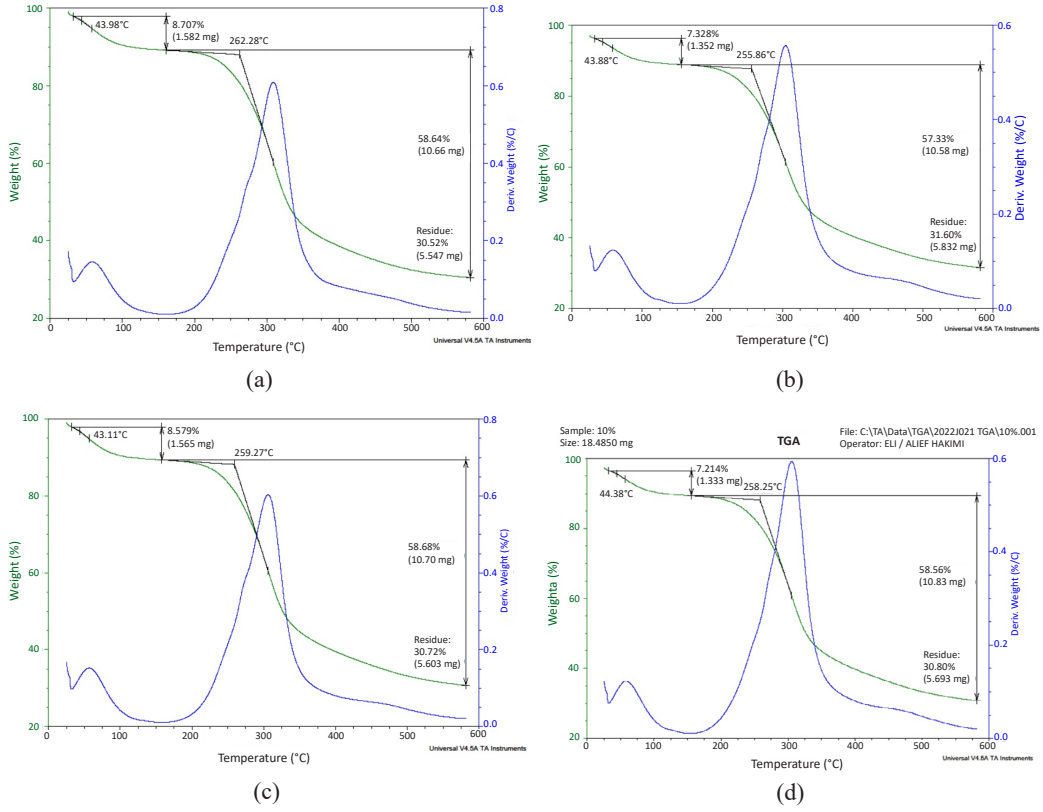

Figure 9. TGA and DTG curves of DSF/PMDI boards for (a) 0, (b) 6, (c) 8 and (d) 10% of PMDI

weight loss describes cellulosic component degradation that occurs largely in amorphous areas to eliminate water molecules at 43-60°C (Ramlee et al., 2021).

The best thermal stability can be expressed as high initial and final temperatures and a high content of char residue (Chee et al., 2019). Based on Table 3, it can be concluded that DSF/6PMDI has the best thermal stability compared to other composites due to the lowest weight loss and highest char residue. When the temperature increased, the final

degradation temperature for DSF/6PMDI was the lowest due to the weak thermal stability of the composite. It may be supported by the fact that the thermal degradation of cellulosic material, consisting of cellulose, hemicellulose, and lignin, is initiated at temperatures around 200 to 400°C (Aimi et al., 2015). Cellulose started decomposing at the highest temperature for second mass loss as it has the highest thermal stability compared to lignin and hemicellulose. This reason is related to cellulose having more crystalline chains than amorphous ones in their structure (Chee et al., 2019). DSF/6PMDI had the highest (31.6%) char residue at 580°C related to highly condensed aromatic structure involvement.

The DTG curves in Figure 9 are crucial as they help determine the maximum temperature for the weight loss step. The secondary weight loss involving thermal degradation of hemicellulose followed by cellulose and lignin was initiated at 250–310ºC (Koay et al., 2018). The percentage of charred residue improved as the lignin percentage of the composite improved. Due to the aromatic components of PMDI, using a PMDI compatibiliser contributed to a modest increase in the percentage of charred residues in the composites (Sahoo et al., 2011). This outcome reflects lignin is flame-resistant ability, further boosted by PMDI addition. The increment in this ability will increase the percentage of char residue. Increasing the char residue will reduce the combustible gases and, at the same time, will save the environment (Shih et al., 2006). These outcomes were similar to the research, which indicated that 6% was the optimum content of PMDI incorporated into kenaf fibre-reinforced thermoplastic polyurethane composites that produced less weight loss and high thermal stability (El-Shekeil et al., 2012).

Differential Scanning Calorimetry Analysis

Differential scanning calorimetry (DSC) is a standard approach for polymer analysis, which strengthens our understanding of the microphase structure when combined with other supporting methods. DSC has been used to identify the materials' phase transition, which could be exothermic or endothermic. For all samples, it was observed that there were similar patterns of profiles, which include double endothermic process and single exothermic. The first indicates the glass transition phase, the second indicates the melting phase for the endothermic process, and the exothermic process shows the cold crystallisation process. Through DSC, the other important thermal properties such as glass transition temperature (T_g), melting temperature (T_m), cold crystallisation temperature (T_c), crystallisation entropy (ΔH_c), and melting entropy (ΔH_m) can be achieved based on Figure 10. Table 4 shows the summary of the DSC test for the boards.

Glass Transition Phase. The T_g in each graph for composites indicates that the energy needed to transition the molecular structure within the composites from a low energy state, such as a solid or glassy state, to a higher energy level, such as a rubbery state, is specified

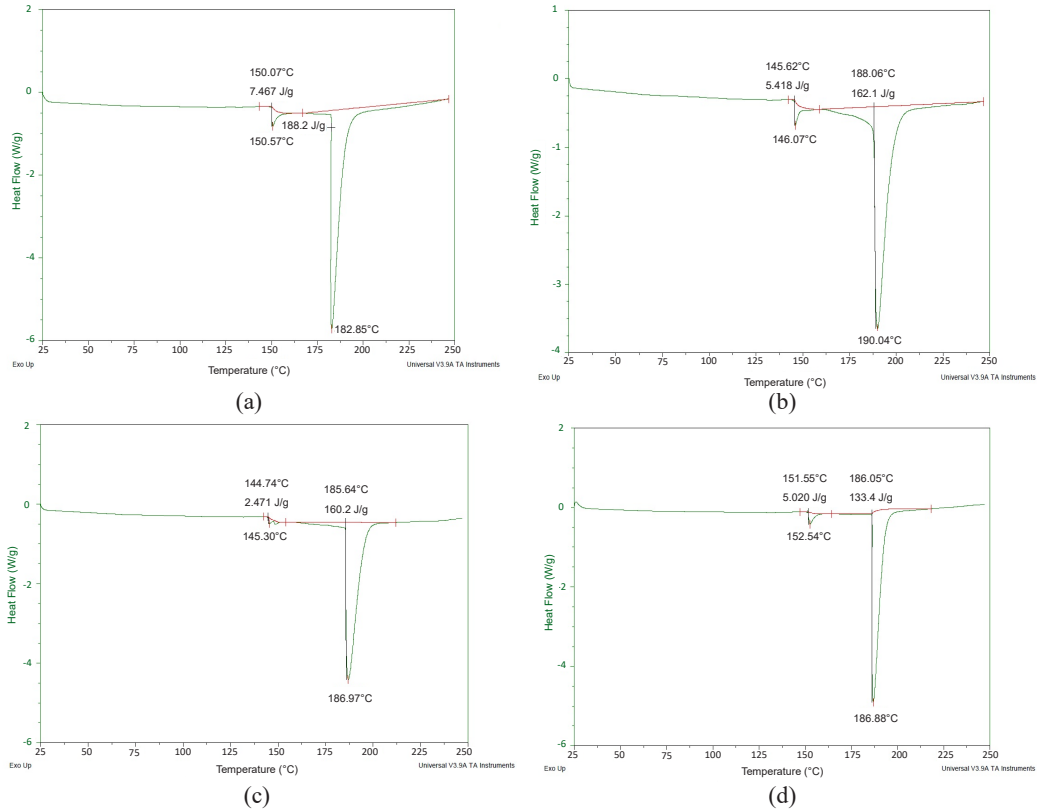

Figure 10. DSC curves of DSF/PMDI boards for (a) 0, (b) 6, (c) 8, and (d) 10% of PMDI.

Table 4
Summary of DSC test findings for the DSF/PMDI boards

Sample	T_g onset (°C)	T_g peak (°C)	T_c peak (°C)	ΔH_c (J/g)	T_m onset (°C)	T_m peak (°C)	ΔH_m (J/g)
DSF/0PMDI	150.07	150.57	163.60	4.603	182.85	182.85	188.2
DSF/6PMDI	145.62	146.07	160.27	1.102	188.06	190.04	162.1
DSF/8PMDI	144.74	145.30	147.20	0.665	185.64	186.97	160.2
DSF/10PMDI	151.55	152.54	165.88	0.643	186.05	186.88	133.4

as the starting point. By comparing the T_g for the composites, DSF/10PMDI has the highest value, which is 152.54°C, followed by DSF/0PMDI (150.57°C), DSF/6PMDI (146.07°C), and DSF/8PMDI (145.30°C). At this phase, polymer chains modify their molecular system to convert from amorphous to crystalline solid by gradually organising their structures (Aisyah et al., 2019). Since the glass transition temperature is higher, a higher temperature is required to change the sample from a glass to a rubbery condition (Azlin et al., 2022).

The glass transition temperature was also modified when the PMDI concentration was raised. A polymer-filler interaction and plasticisation triggered by PMDI addition might be regarded as the potential explanations of the findings reported in this work, although the impact on the thermal properties of natural fibre composites incorporated with PMDI is not very clear (Sahoo et al., 2011).

Cold Crystallisation Phase

Continuous heating of the composites led to the exothermic process known as cold crystallisation, in which the composites change from glassy to an amorphous state (Azlin et al., 2022). It happens between the glass transition and melting phases, which takes place in the 140–170°C range for all the composites. By comparing the T_c for the composites, DSF/10PMDI has the highest value, which is 165.88°C followed by DSF/0PMDI (163.60°C), DSF/6PMDI (160.27°C), and DSF/8PMDI (147.20°C).

Melting Phase. Apart from that, DSF/6PMDI have the highest value, which is 190.04°C, followed by DSF/8PMDI (186.97ºC), DSF/10PMDI (186.88°C), and DSF/0PMDI (182.85°C) after comparing their value of T_m. It can be considered the optimum concentration of PMDI as T_m was increased after DSF had been incorporated with 6% of PMDI content and then decreased with 8 and 10%. This trend also has similarities with the research by El-Shekeil et al. (2012), where they introduced PMDI into kenaf fibre-reinforced thermoplastic polyurethane composites, and the optimum concentration of PMDI was 6%. This alteration in melting temperature signifies an alteration in molecular mobility, such as an alteration in the interfacial adhesion of fibre and polymer. Consequently, the availability of stacking or intermolecular bonding in composites may explain the different content of PMDI, which led to the alteration of the value of T_m.

ΔH_m value is also important as it is associated with the degree of crystallinity of the polymer itself (Manshor et al., 2014). It can be assumed that DSF/0PMDI had the highest degree of crystallinity compared to others as it has the highest value of ΔH_m. The addition of PMDI reduced the crystallinity of composites, and its further decrement was found with the rising concentration of PMDI. Apart from that, there was a large endothermic peak that may be caused by chemical components in natural fibres beginning to degrade at around 200°C (Aisyah et al., 2019). The high peaks for this endothermic indicate that more heat was required to break the polymer chains in composites, and these peaks decreased with increasing concentration of PMDI. In other words, the fibre–matrix interaction modification occurred when the melting temperature changed. As a result, the effect of various percentages of the PMDI additive may be correlated with stacking or intermolecular bonding in composites (El-Shekeil et al., 2012).

Dynamic Mechanical Analysis

Dynamic mechanical analysis (DMA) is a technique that employs a sinusoidal load on a specimen and evaluates the resulting deformation while the sample is exposed to a set temperature program to determine the material's stiffness and damping qualities. The method is especially effective for assessing the influence of moisture on T_g. Table 5 summarises the DMA test OF DSF/PMDI boards. The 0% of the PMDI sample did not undergo this test due to the failure to get below 6 mm of thickness during the sampling process, as the thickness is a crucial requirement for the testing.

Storage Modulus. Figure 11 shows storage modulus curves for all the boards. The storage modulus value decreased with the rising temperature and increasing concentration of PMDI. The decline in storage modulus with temperature may be related to the polymer matrix's enhanced chain mobility at high temperatures, which softens the polymer (Sahoo et al., 2011). During the phase preceding T_g (glassy state), the densely packed molecules caused the composite structure to become extremely stiff and rigid due to the high rigidity of the polymeric chain. In the glass transition phase, it was discovered that the storage modulus fell above T_g, attributable to polymeric chain movement. The movement of polymeric chains influenced both the stiffness and interfacial adhesion. During the third phase (rubbery state), which preceded the glass transition phase, there was no big difference in storage modulus due to increased polymeric chain mobility at elevated temperatures (Jesuarockiam et al., 2019).

DSF/6PMDI achieved the lowest storage modulus values compared to other samples, and the value of storage modulus increased as the concentration of PMDI increased. The decreasing value of the storage modulus represents the decreasing stiffness value for the material (Chee et al., 2019). Storage modulus decreases as temperature increases attributable to chain mobility in the polymer matrix, which leads to the polymer being softer and less rigid and also may happen due to the strengthening of fibres within the composites (Azlin et al., 2022; Sahoo et al., 2011). The amorphous phase may limit chain mobility, reducing the composite's stiffness (Aimi et al., 2015).

Table 5
Summary of DMA test for the DSF/PMDI boards

Sample	T_g Onset—Storage Modulus (°C)	T_g Peak—Loss Modulus (°C)	T_g Peak—Tan Delta (°C)
DSF/6PMDI	82.79	90.48	98.42
DSF/8PMDI	67.89	84.76	100.38
DSF/10PMDI	47.25	67.03	78.79

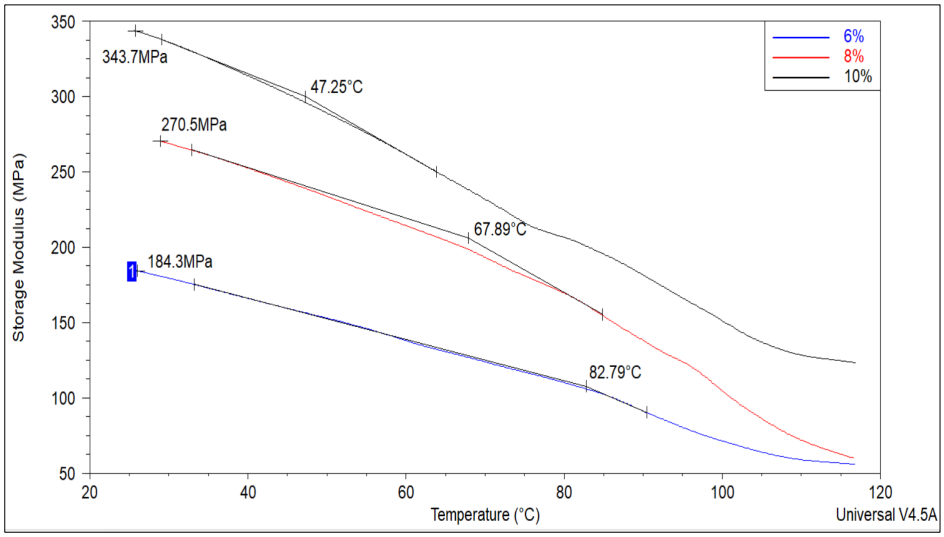

Figure 11. Storage modulus curves for DSF/PMDI boards

Loss Modulus. Figure 12 shows loss modulus curves for all the composites. Based on the figure, DSF/6PMDI has the lowest loss modulus value compared to other composites. The increasing value of loss modulus represents the viscous and damping qualities of the material (Chee et al., 2019). It can be considered that DSF/0PMDI had the lowest loss modulus as it was not strong enough and brittle. The loss modulus measures the material's viscous component to its complex modulus. In the glass transition area, the loss modulus gained a maximum peak, reflecting a large amount of energy loss related to the internal friction and non-elastic deformation in the molecular segmental motion (Chee et al., 2019). The glass transition phase in all composites occurred in a temperature region starting from 60 until 100°C. The T_g started happening when the storage modulus dropped quickly, and the loss modulus reached its maximum value for the loss of mechanical energy. At higher temperatures, the free movement of the polymeric chain caused the loss modulus to fall (Nurazzi et al., 2021).

The value of the T_g can be observed from the graph by observing the peak of the profiles. The T_g value obtained from the peak value of loss modulus stated that DSF/6PMDI had the highest value of 90.48°C, followed by DSP/8PMDI (84.76°C), and then DSF/10PMDI (67.03°C). The T_g obtained from the peak of loss modulus shows that the value decreased with the increasing content of PMDI. The increasing content exceeding 6% decreased the glass transition temperature. The greater the value of T_g, the stronger the interface connection between the fibres and the matrix (Nurazzi et al., 2021).

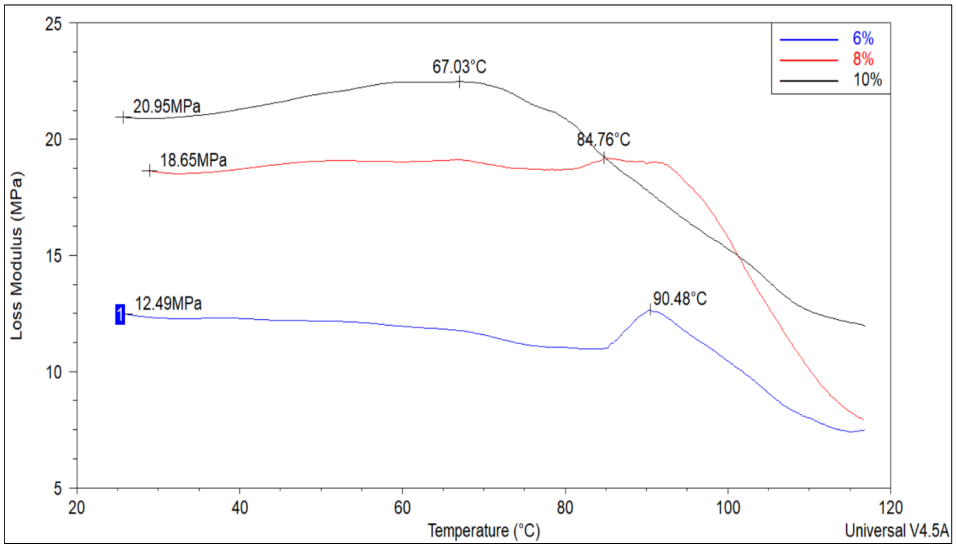

Figure 12. Loss modulus curves for DSF/PMDI boards

Damping Factor (Tan Delta). Figure 13 shows tan delta curves for all the boards. A similar trend can be observed in the graph of the tan delta, which shows an increasing damping factor with increasing temperature for all boards, and this happened due to the chain segments becoming more mobile as the temperature goes up, resulting in a higher value for damping factor (Mohammed et al., 2017). By observing the graph of the tan delta, the highest value was achieved by 8% (100.38°C), followed by 6% (98.42°C) and then 10% (78.79°C) (103.06). The highest value indicates the T_g for the composites. Apart from that, the low damping factor indicates that adhesion related to the filler and fibre matrix was good and, thus, restricted the mobility of polymer chains (Razali et al., 2021). In this case, the increasing content of PMDI decreased the value of tan delta, thus producing good interface adhesion between the natural fibre matrix and PMDI resin. The decreasing value of tan delta was also directly proportional to the value of T_g, indicating the increasing value of interfacial adhesion for the composites (Nurazzi et al., 2021).

There are two explanations for the increasing T_g that need to be appointed. The first reason is due to the formation of an amorphous fraction in the composite structure in which the polymer and filler coexisted in a tightly linked form, thus lowering the free volume of the composites and increasing their T_g. Possible secondary bonds that operate as quasi-crosslinks and constrain the Brownian motion of long-chain molecules may also lead to a rise in T_g (Sahoo et al., 2011). The T_g for composites increased to 8% and then rapidly decreased for 10% of PMDI concentration. The decreasing T_g of 10% is due to the plasticisation of the materials that create free volume between interfacial adhesion of the composites, thus decreasing the T_g (Hetayothin, 2010). Another possible reason for

increasing T_g is regarding the density of composites. DSF/8PMDI have the highest value of density, followed by DSF/6PMDI, DSF/10PMDI and then DSP/0PMDI. The increasing density value indicates that interfacial adhesion also increased due to smaller pores and thus increased the T_g (Mandal & Alam, 2012).

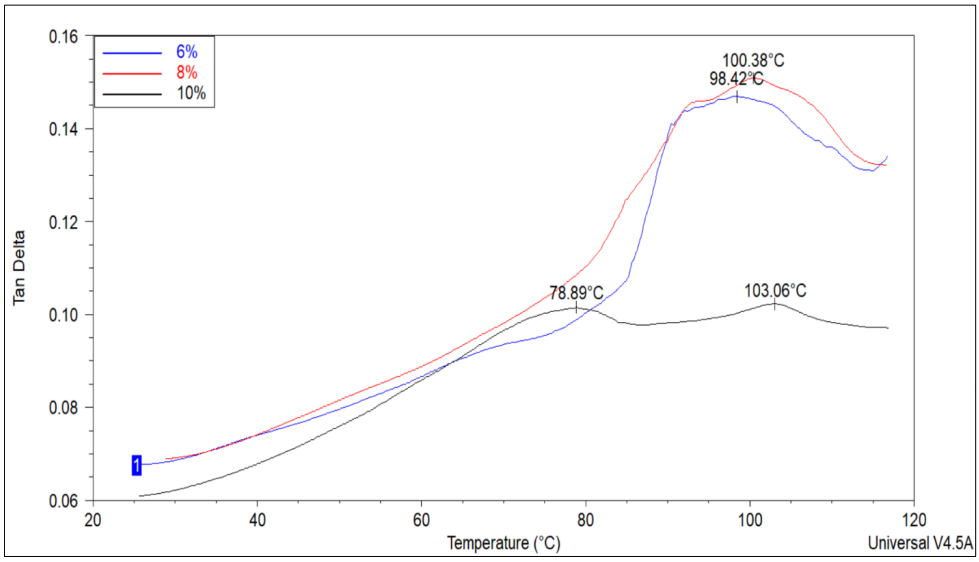

Figure 13. Tan delta curves for DSF/PMDI boards

Thermal Conductivity Measurement

Thermal conductivity measurements are highly related to heat transfer as thermal conductivity is inversely proportional to thermal resistance (Corumlu et al., 2018). Thermal conductivity value for the insulation materials is crucial as it could be the key factor in choosing the suitable composites used as an insulator in the building. In other words, the lowest thermal conductivity value will be concluded as the best composite for the insulation purpose. It also shows that the heat will flow slower when the conductivity value is minimal (Ramlee et al., 2021). Based on Figure 16, it can be said that DSF/0PMDI had the lowest value for thermal conductivity of 0.07892 W/m.k, followed by DSF/6PMDI (0.08275 W/m.K), DSF/10PMDI (0.08694 W/m.K), and then DSF/8PMDI(0.08940 W/m.K).

Based on Figure 2, DSF/0PMDI exhibited the lowest density, while DSF/8PMDI had the highest density compared to other composites. These values of thermal conductivity are directly proportional to the board density. In other words, the increasing value of density resulted in the increasing value of thermal conductivity (Khedari et al., 2003; Luamkanchanaphan et al., 2012). The structure of the boards has several voids, although it seems solid in its appearance. Void positions in the fibres are inversely related

to board density. The air inside the voids decreases the thermal conductivity value (Luamkanchanaphan et al., 2012). In addition, it is strongly suggested to utilise natural fibres such as DSF, which contain cellulose, hemicellulose, and lignin that are bound together to serve as a heat barrier (Ibraheem et al., 2011b).

Apart from that, by comparing the value of thermal conductivity from multiple types of materials, DSF/PMDI composites achieved the standard with other materials such as oil palm (0.055 W/m.K) (Manohar, 2012), coconut husk (0.046 W/m.K) (Panyakaew & Fotios, 2011), and durian combine with coconut coir (0.064 W/m.K) (Khedari et al., 2003). Furthermore, all samples' thermal conductivity values were below 0.1 W/m.K, indicating excellent thermal insulation materials (Ramlee et al., 2021). Figure 14 shows the thermal conductivity, while Figure 15 displays the thermal resistance of the boards.

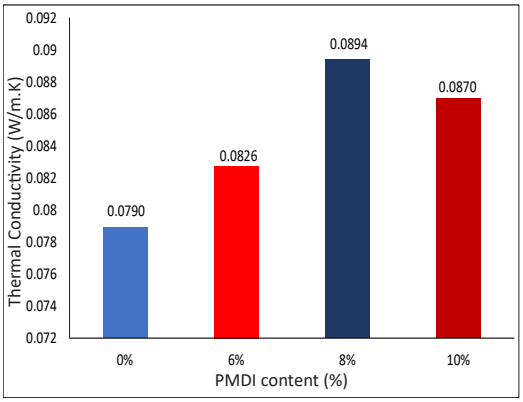

Figure 14. Thermal conductivity of the DSF/PMDI boards

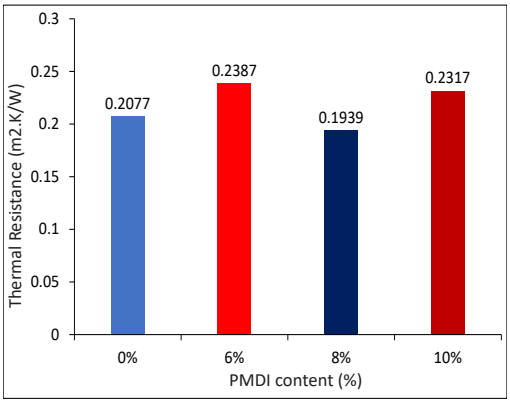

Figure 15. Thermal resistance of the DSF/PMDI boards

Furthermore, thermal resistance is one of the most important factors in choosing the best insulation materials. The higher thermal resistance value indicates that the material has excellent insulation quality. Based on the values that were achieved and presented in Figure 15, DSF/6PMDI gave the highest value of thermal resistance, which is 0.2387 m^2K/W, followed by DSF/10PMDI, DSF/0PMDI, and DSF/8PMDI.

CONCLUSION

The findings suggest that incorporating durian waste can be an alternative solution for utilising the waste management problem. The resin content affects all the board properties. The insulation board with 6% PMDI content resulted in ideal mechanical and thermal properties. Low resin content produced board with excellent all-bending properties, good bonding properties, high thermal stability, and good thermal conductivity compared to other composites. Overall, the DSF/6PMDI board has better board properties, particularly their

mechanical properties, as the MOE and MOR are the most crucial aspects in developing an insulation board and the thermal properties. It also cut the cost of producing the board as the low resin was used. Although it has average dimensional stability, the board can be covered using a waterproof coating. Nonetheless, the potential uses of these boards have enabled the use of agricultural waste composites in construction and building applications.

ACKNOWLEDGEMENTS

The authors are grateful to acknowledge Noorashikin Soh binti Zulariffin Soh and Aleif Hakimi bin Ismail of Universiti Putra Malaysia for help in collecting the data.

REFERENCES

Adunphatcharaphon, S., Petchkongkaew, A., Greco, D., D'Ascanio, V., Visessanguan, W., & Avantaggiato, G. (2020). The effectiveness of durian peel as a multi-mycotoxin adsorbent. *Toxins*, *12*(2), 108. https://doi.org/10.3390/toxins12020108

Aimi, M. N., Anuar, H., Maizirwan, M., Sapuan, S. M., Wahit, M. U., & Zakaria, S. (2015). Preparation of durian skin nanofibre (DSNF) and its effect on the properties of polylactic acid (PLA) biocomposites. *Sains Malaysiana*, *44*(11), 1551-1559.

Aimi, N. N., Anuar, H., Manshor, M. R., Nazri, W. W., & Sapuan, S. M. (2014). Optimizing the parameters in durian skin fibre reinforced polypropylene composites by response surface methodology. *Industrial Crops and Products*, *54*, 291-295. https://doi.org/10.1016/j.indcrop.2014.01.016

Aisyah, H. A., Paridah, M. T., Sapuan, S. M., Khalina, A., Berkalp, O. B., Lee, S. H., Lee, C. H., Nurazzi, N. M., Ramli, N., Wahab, M. S. & Ilyas, R. A. (2019). Thermal properties of woven kenaf/carbon fibre-reinforced epoxy hybrid composite panels. *International Journal of Polymer Science*, *2019*, 1-8. https://doi.org/10.1155/2019/5258621

Alamri, H., & Low, I. M. (2012). Mechanical properties and water absorption behaviour of recycled cellulose fibre reinforced epoxy composites. *Polymer Testing*, *31*(5), 620-628. https://doi.org/10.1016/j.polymertesting.2012.04.002

Ali, A., Shaker, K., Nawab, Y., Jabbar, M., Hussain, T., Militky, J., & Baheti, V. (2018). Hydrophobic treatment of natural fibers and their composites—A review. *Journal of Industrial Textiles*, *47*(8), 2153-2183. https://doi.org/10.1177/15280837166544

Ali, A., Shaker, K., Nawab, Y., Ashraf, M., Basit, A., Shahid, S., & Umair, M. (2015). Impact of hydrophobic treatment of jute on moisture regain and mechanical properties of composite material. *Journal of Reinforced Plastics and Composites*, *34*(24), 2059-2068. https://doi.org/10.1177/0731684415610007

Alomayri, T., Assaedi, H., Shaikh, F. U. A., & Low, I. M. (2014). Effect of water absorption on the mechanical properties of cotton fabric-reinforced geopolymer composites. *Journal of Asian Ceramic Societies*, *2*(3), 223-230. https://doi.org/10.1016/j.jascer.2014.05.005

Asyraf, M. R. M., Syamsir, A., Ishak, M. R., Sapuan, S. M., Nurazzi, N. M., Norrrahim, M. N. F., Ilyas, R. A., Khan, T., & Rashid, M. Z. A. (2023). Mechanical properties of hybrid lignocellulosic fiber-reinforced biopolymer green composites: A review. *Fibers and Polymers*, *24*(2), 337-353. https://doi.org/10.1007/s12221-023-00034-w

Asyraf, M. R. M., Nurazzi, N. M., Norrrahim, M. N. F., Hazrati, K. Z., Ghani, A., Sabaruddin, F. A., Lee, S. H., Shazleen, S. S., & Razman, M. R. (2023). Thermal properties of oil palm lignocellulosic fibre reinforced polymer composites: A comprehensive review on thermogravimetry analysis. *Cellulose*, *30*(5), 2753-2790. https://doi.org/10.1007/s10570-023-05080-4

Asyraf, M. R. M., Rafidah, M., Ebadi, S., Azrina, A., & Razman, M. R. (2022). Mechanical properties of sugar palm lignocellulosic fibre reinforced polymer composites: A review. *Cellulose*, *29*(12), 6493-6516. https://doi.org/10.1007/s10570-022-04695-3

ASTM D1895. (2003). *Standard test methods for direct moisture content measurement of wood and wood-base materials*. ASTM International. https://www.astm.org/d4442-92r03.html

ASTM E1640. (2018). *Standard test method for assignment of the glass transition temperature by dynamic mechanical analysis*. ASTM International. https://www.astm.org/e1640-18.html

ASTM D1037. (2020). *Standard test methods for evaluating properties of wood-base fibre and particle panel materials.* ASTM International. https://www.astm.org/d1037-12r20.html

ASTM E1131. (2020). *Standard test method for compositional analysis by thermogravimetry* ASTM International. https://www.astm.org/e1131-20.html

ASTM C518. (2021). *Standard test method for steady-state thermal transmission properties by means of the heat flow meter apparatus*. ASTM International. https://www.astm.org/c0518-21.html

ASTM D3418. (2021). *Standard test method for transition temperatures and enthalpies of fusion and crystallization of polymers by differential scanning calorimetry*. ASTM International. https://www.astm.org/d3418-21.html

ASTM D2395. (2022). *Standard test methods for density and specific gravity (relative density) of wood and wood-based materials*. ASTM International. https://www.astm.org/d2395-17r22.html

Azammi, A. N., Ilyas, R. A., Sapuan, S. M., Ibrahim, R., Atikah, M. S. N., Asrofi, M., & Atiqah, A. (2020). Characterization studies of biopolymeric matrix and cellulose fibres based composites related to functionalized fibre-matrix interface. In Interfaces in particle and fibre reinforced composites (pp. 29-93). Woodhead Publishing. https://doi.org/10.1016/B978-0-08-102665-6.00003-0

Azlin, M. N. M., Sapuan, S. M., Zuhri, M. Y. M., Zainudin, E. S., & Ilyas, R. A. (2022). Thermal stability, dynamic mechanical analysis and flammability properties of woven kenaf/polyester-reinforced polylactic acid hybrid laminated composites. *Polymers*, *14*(13), 2690. https://doi.org/10.3390/polym14132690

Azman, M. A., Asyraf, M. R. M., Khalina, A., Petrů, M., Ruzaidi, C. M., Sapuan, S. M., Wan Nik, W. B., Ishak, M. R., Ilyas, R. A., & Suriani, M. J. (2021). Natural fiber reinforced composite material for product design: A short review. *Polymers*, *13*(12), 1917. https://doi.org/10.3390/polym13121917

Chee, S. S., Jawaid, M., Sultan, M. T. H., Alothman, O. Y., & Abdullah, L. C. (2019). Accelerated weathering and soil burial effects on colour, biodegradability and thermal properties of bamboo/kenaf/epoxy hybrid composites. *Polymer Testing*, *79*, 106054. https://doi.org/10.1016/j.polymertesting.2019.106054

Corumlu, V., Ozsoy, A., & Ozturk, M. (2018). Fabrication and investigation of silver water nanofluids for long-term heat transfer application. In I. Dincer., C. Ozgur Colpan., & O. Kizilkan (Eds.), *Exergetic, energetic and environmental dimensions* (pp. 779-791). Academic Press. https://doi.org/10.1016/B978-0-12-813734-5.00044-5

E'zzati, M. S. N., Anuar, H., & Salimah, A. S. M. (2018). Effect of coupling agent on durian skin fibre nanocomposite reinforced polypropylene. *IOP Conference Series: Materials Science and Engineering, 290*(1), 012032. https://doi.org/ 10.1088/1757-899X/290/1/012032

El-Shekeil, Y. A., Sapuan, S. M., Abdan, K., Zainudin, E. S., & Al-Shuja'a, O. M. (2012). Effect of pMDI isocyanate additive on mechanical and thermal properties of kenaf fibre reinforced thermoplastic polyurethane composites. *Bulletin of Materials Science*, *35*(7), 1151-1155.

Hetayothin, B. (2010). Effect of structure and plasticizer on the glass transition of adsorbed polymer [Doctoral dissertation, Missouri University of Science and Technology]. Missouri University of Science and Technology. https://scholarsmine.mst.edu/doctoral_dissertations/1901/

Ho, L. H., & Bhat, R. (2015). Exploring the potential nutraceutical values of durian (*Durio zibethinus* L.)–An exotic tropical fruit. *Food Chemistry*, *168*, 80-89. https://doi.org/10.1016/j.foodchem.2014.07.020

Ibraheem, S. A., Ali, A., & Khalina, A. (2011). Development of green insulation boards from kenaf fibres and polyurethane. *Polymer-plastics Technology and Engineering*, *50*(6), 613-621. https://doi.org/10.1080/03602559.2010.551379

Jani, S. M., & Izran, K. (2013). Mechanical and physical properties of ureaformaldehyde bonded kenaf core particle boards. *Journal of Tropical Agriculture and Food Science*, *41*(2), 341-347.

Jesuarockiam, N., Jawaid, M., Zainudin, E. S., Thariq Hameed Sultan, M., & Yahaya, R. (2019). Enhanced thermal and dynamic mechanical properties of synthetic/natural hybrid composites with graphene nanoplateletes. *Polymers*, *11*(7), 1085. https://doi.org/10.3390/polym11071085

Khedari, J., Charoenvai, S., & Hirunlabh, J. (2003). New insulating particleboards from durian peel and coconut coir. *Building and Environment*, *38*(3), 435-441. https://doi.org/10.1016/S0360-1323(02)00030-6

Khedari, J., Nankongnab, N., Hirunlabh, J., & Teekasap, S. (2004). New low-cost insulation particleboards from mixture of durian peel and coconut coir. *Building and Environment*, *39*(1), 59-65. https://doi.org/10.1016/j.buildenv.2003.08.001

Koay, S. C., Subramanian, V., Chan, M. Y., Pang, M. M., Tsai, K. Y., & Cheah, K. H. (2018). Preparation and characterisation of wood plastic composite made up of durian husk fibre and recycled polystyrene foam. *MATEC Web of Conferences*, *152*, 02019. https://doi.org/10.1051/matecconf/201815202019

Kusumah, S. S., Umemura, K., Guswenrivo, I., Yoshimura, T., & Kanayama, K. (2017). Utilisation of sweet sorghum bagasse and citric acid for manufacturing of particleboard II: influences of pressing temperature and time on particleboard properties. *Journal of Wood Science*, *63*(2), 161-172.

Liu, R., Long, L., Sheng, Y., Xu, J., Qiu, H., Li, X., Wang, Y., & Wu, H. (2019). Preparation of a kind of novel sustainable mycelium/cotton stalk composites and effects of pressing temperature on the properties. *Industrial Crops and Products*, *141*, 111732. https://doi.org/10.1016/j.indcrop.2019.111732

Luamkanchanaphan, T., Chotikaprakhan, S., & Jarusombati, S. (2012). A study of physical, mechanical and thermal properties for thermal insulation from narrow-leaved cattail fibres. *APCBEE Procedia*, *1*, 46-52. https://doi.org/10.1016/j.apcbee.2012.03.009

Mandal, S., & Alam, S. (2012). Dynamic mechanical analysis and morphological studies of glass/bamboo fibre reinforced unsaturated polyester resin-based hybrid composites. *Journal of Applied Polymer Science*, *125*(S1), E382-E387. https://doi.org/10.1002/app.36304

Manohar, K. (2012). Experimental investigation of building thermal insulation from agricultural by-products. *British Journal of Applied Science & Technology*, *2*(3), 227-239.

Manshor, M. R., Anuar, H., Aimi, M. N., Fitrie, M. A., Nazri, W. W., Sapuan, S. M., El-Shekeil, Y. A., & Wahit, M. U. (2014). Mechanical, thermal and morphological properties of durian skin fibre reinforced PLA biocomposites. *Materials & Design*, *59*, 279-286. https://doi.org/10.1016/j.matdes.2014.02.062

Manshor, R. M., Anuar, H., Wan Nazri, W. B., & Fitrie, M. I. (2012). Preparation and characterisation of physical properties of durian skin fibres biocomposite. *Advanced Materials Research*, *576*, 212-215. https://doi.org/10.4028/www.scientific.net/AMR.576.212

Masrifah, A., Setyaningrum, H., Susilo, A., & Haryadi, I. (2021). Perancangan Sistem Pengelolaan Limbah Durian Layak Kompos Di Agrowisata Kampung Durian Ponorogo. *Engagement: Jurnal Pengabdian Kepada Masyarakat*, *5*(1), 268-282.

Mohammed, B. R., Leman, Z., Jawaid, M., Ghazali, M. J., & Ishak, M. R. (2017). Dynamic mechanical analysis of treated and untreated sugar palm fibre-based phenolic composites. *BioResources*, *12*(2), 3448-3462.

Mossello, A. A., Harun, J., Shamsi, S. R. F., Resalati, H., Tahir, P. M., Rushdan, I., & Mohmamed, A. Z. (2010). A review of literatures related to kenaf as a alternative for pulpwoods. *Agricultural Journal*, *5*(3), 131-138.

Nazri, W., Ezdiani, Z., Romainor, M., Erma, K. S., Jurina, J., & Fadzlina, I. N. (2014). Effect of fibre loading on mechanical properties of durian skin fibre composite. *Journal of Tropical Agricultural Food Science*, *42*(2), 169-174.

Norfarhana, A. S., Ilyas, R. A., & Ngadi, N. (2022). A review of nanocellulose adsorptive membrane as multifunctional wastewater treatment. *Carbohydrate Polymers*, Article 119563. https://doi.org/10.1016/j.carbpol.2022.119563.

Nurazzi, N. M., Norli, A., Norrrahim, M. N. F., Rafiqah, S. A., Khalina, A., Sapuan, S. M., & Ilyas, R. A. (2021). Thermal properties of sugar palm yarn reinforced unsaturated polyester composites as an alternative for automotive applications. In S. M., Sapuan., & R. A., Ilyas (Eds.) *Biocomposite and synthetic composites for automotive applications* (pp. 19-49). Woodhead Publishing.

Ostendorf, K., Ahrens, C., Beulshausen, A., Tene Tayo, J. L., & Euring, M. (2021). On the feasibility of a pMDI-reduced production of wood fibre insulation boards by means of kraft lignin and ligneous canola hulls. *Polymers*, *13*(7), 1088. https://doi.org/10.3390/polym13071088

Panyakaew, S., & Fotios, S. (2011). New thermal insulation boards made from coconut husk and bagasse. *Energy and Buildings*, *43*(7), 1732-1739. https://doi.org/10.1016/j.enbuild.2011.03.015

Payus, C. M., Refdin, M. A., Zahari, N. Z., Rimba, A. B., Geetha, M., Saroj, C., Gasparatos, A., Fukushi, K., & Oliver, P. A. (2021). Durian husk wastes as low-cost adsorbent for physical pollutants removal: Groundwater supply. *Materials Today: Proceedings*, *42*(1), 80-87. https://doi.org/10.1016/j.matpr.2020.10.006

Penjumras, P., Rahman, R. A., Talib, R. A., & Abdan, K. (2015). Mechanical properties and water absorption behaviour of durian rind cellulose reinforced poly (lactic acid) biocomposites. *International Journal on Advanced Science, Engineering and Information Technology*, *5*(5), 343-349.

Ramlee, N. A., Jawaid, M., Ismail, A. S., Zainudin, E. S., & Yamani, S. A. K. (2021). Evaluation of thermal and acoustic properties of oil palm empty fruit bunch/sugarcane bagasse fibres based hybrid composites for wall buildings thermal insulation. *Fibres and Polymers*, *22*(9), 2563-2571.

Razali, N., Sultan, M. T. H., Shah, A. U. M., & Safri, S. N. A. (2021). Low velocity impact characterisation of flax/kenaf/glass fibre reinforced epoxy hybrid composites. In M. Thariq Hameed Sultan, A. U., Md Shah., & N., Saba (Eds.) *Impact Studies of Composite Materials* (pp. 195-208). Springer.

Saad, M. J., & Kamal, I. (2012). Mechanical and physical properties of low density kenaf core particleboards bonded with different resins. *Journal of Science and Technology*, *4*(1), 17-32.

Sabaruddin, F. A., Paridah, M. T., Sapuan, S. M., Ilyas, R. A., Lee, S. H., Abdan, K., Mazlan, N., Roseley, A. S. M., & Khalil, H. P. S. (2020). The effects of unbleached and bleached nanocellulose on the thermal

and flammability of polypropylene-reinforced kenaf core hybrid polymer bionanocomposites. *Polymers*, *13*(1), 116. https://doi.org/10.3390/polym13010116.

Sahoo, S., Misra, M., & Mohanty, A. K. (2011). Enhanced properties of lignin-based biodegradable polymer composites using injection moulding process. *Composites Part A: Applied Science and Manufacturing*, *42*(11), 1710-1718. https://doi.org/10.1016/j.compositesa.2011.07.025

San Ha, N., Lu, G., Shu, D., & Yu, T. X. (2020). Mechanical properties and energy absorption characteristics of tropical fruit durian (*Durio zibethinus*). *Journal of the Mechanical Behaviour of Biomedical Materials*, *104*, 103603. https://doi.org/10.1016/j.jmbbm.2019.103603

Sargent, R. (2019). Evaluating dimensional stability in solid wood: A review of current practice. *Journal of Wood Science*, *65*(1), 1-11.

Shaker, K., Umair, M., Shahid, S., Jabbar, M., Ullah Khan, R. M. W., Zeeshan, M., & Nawab, Y. (2022). Cellulosic fillers extracted from *Argyreia speciose* waste: a potential reinforcement for composites to enhance properties. *Journal of Natural Fibers*, *19*(11), 4210-4222. https://doi.org/10.1080/15440478.2020.1856271

Shaker, K., Khan, R. M. W. U., Jabbar, M., Umair, M., Tariq, A., Kashif, M., & Nawab, Y. (2020). Extraction and characterization of novel fibers from *Vernonia elaeagnifolia* as a potential textile fiber. *Industrial Crops and Products*, *152*, 112518. https://doi.org/10.1016/j.indcrop.2020.112518

Shih, Y. F., Lee, W. C., Jeng, R. J., & Huang, C. M. (2006). Water bamboo husk-reinforced poly (butylene succinate) biodegradable composites. *Journal of Applied Polymer Science*, *99*(1), 188-199. https://doi.org/10.1002/app.22220

Wong, E. D., Zhang, M., Han, G., Kawai, S., & Wang, Q. (2000). Formation of the density profile and its effects on the properties of fibreboard. *Journal of Wood Science*, *46*(3), 202-209.

Yousefi, J., Mohamadi, R., Saeedifar, M., Ahmadi, M., & Hosseini-Toudeshky, H. (2016). Delamination characterisation in composite laminates using acoustic emission features, micro visualization and finite element modeling. *Journal of Composite Materials*, *50*(22), 3133-3145. https://doi.org/10.1177/00219983156156

Yuan, C., Chen, W., Pham, T. M., & Hao, H. (2019). Effect of aggregate size on bond behaviour between basalt fibre reinforced polymer sheets and concrete. *Composites Part B: Engineering*, *158*, 459-474. https://doi.org/10.1016/j.compositesb.2018.09.089

Zakaria, A. A. (2020). *Managing Durian Orchards in Malaysia*. Universiti Putra Malaysia Press.